

---

# Attenuation Correction in SPECT Based on Transmission Studies and Monte Carlo Simulations of Build-Up Functions

Michael Ljungberg and Sven-Erik Strand

*Radiation Physics Department, University of Lund, Sweden*

---

The quantitative information in SPECT images is distorted by photon attenuation and contribution of photons scattered in the object. It is, therefore, important to know the distribution of different attenuating tissues in order to be able to perform a proper attenuation correction. A correction method, based on correcting one pixel at a time by using density maps and build-up functions, has been developed. The density map has been produced by transmission measurements of the object using an external, solid  $^{57}\text{Co}$  flood source mounted on the scintillation camera head. The outline of the object is accurately defined by the map since the density values outside the object are very close to zero. The build-up of photons scattered in the object has been simulated by a Monte-Carlo code. SPECT-studies with  $^{99\text{m}}\text{Tc}$ ,  $^{201}\text{Tl}$  and  $^{111}\text{In}$  line sources in different parts of a nonhomogeneous Alderson phantom have been performed. The emission images have been corrected for photon attenuation using the measured density maps and the simulated build-up functions. The results show that quantitative measurements of the radioactivity in nonhomogeneous area can be accomplished to within  $\pm 10\%$  for different radionuclides by using the attenuation correction described.

**J Nucl Med 1990; 31:493-500**

---

**T**he quantitative determination of the radioactivity content in tissues is required in both diagnostic and therapeutic nuclear medicine. Planar scintillation camera measurements can be used to estimate the activity in different organs. The drawback with this technique is, however, the lack of information for the variation of radioactivity with depth. The acquired images are, furthermore, distorted by the activity content in overlapping structures, which is a severe problem when applying attenuation corrections for quantitative estimations. Single-photon emission computed tomography (SPECT) is a well established imaging modality that

gives three-dimensional tomographic images of in vivo radioactivity distribution (1,2). The information in the SPECT images is distorted by photon attenuation. Due to the finite energy resolution of the scintillation camera, there also will be photons scattered in the object that result in energy signals which pass the energy discrimination and, thus, contribute to mispositioned events in the image. These effects limit quantitative measurements and result in decreased contrast and blurred edges of the reconstructed activity distribution in the image. Thus, regions with no radioactivity may appear to contain activity.

The correction for photon attenuation in SPECT is complex, since the true outline of the object, the true activity distribution inside the object, and the tissue distribution in the object are usually unknown initially. The photon attenuation can in general be described in mathematical terms by:

$$\Phi(d) = \Phi_0 \cdot B(x, y, z) \cdot \exp\left[-\int_d^0 \frac{\mu(\tau)}{\rho} \cdot \rho(\tau) d\tau\right], \quad (1)$$

where  $\Phi_0$  is the emitted photon fluence in air and  $\Phi$  is the attenuated photon fluence,  $\mu/\rho$  is the mass-attenuation coefficient (tabulated as a function of the photon energy and the atomic number for the material),  $\rho$  is the density of the object, and  $B$  is a complex function describing the build-up in the particular pixel from scattered photons emitted from other source locations in the object (3). The build-up function also depends on the source distribution, energy discrimination settings, the density distribution and tissue composition, the size and shape of the object and the photon energy and is virtually impossible to solve analytically for a nonhomogeneous object. To overcome this complex situation, several approximate methods of attenuation correction for SPECT have been developed (4,5) that use only a single effective attenuation coefficient, that is, the density variation are assumed to be constant in all parts of the object and the build-up of scattered photons is estimated by reducing the magnitude of the attenuation coefficient  $\mu$  to  $\mu_{\text{eff}}$ . The mathematical description of the photon attenuation is then

---

Received Feb. 15, 1989; revision accepted Nov. 2, 1989.  
For reprints contact: Michael Ljungberg, BSc, Radiation Physics Department, Lasarettet, S-221 85 Lund, Sweden.

reduced to:

$$\Phi(d) = \Phi_0 \cdot \exp(-\mu_{\text{eff}}d). \quad (2)$$

A major problem here is the selection of the 'correct' value for the effective attenuation coefficient  $\mu_{\text{eff}}$ . In addition, for regions in the human body with large variations in attenuation, e.g. the thorax, pharynx and pelvic regions, Equation 2 will not accurately correct for photon attenuation since the variation of both the build-up function and the density distribution is significant. A consideration of both the density distribution and tissue composition and the build-up function is necessary for an accurate attenuation correction. The former can be accomplished by making a transmission measurement of the object using either an external flood source mounted on the scintillation camera head or by using data from an x-ray computerized tomography (CT) scanner. The build-up function must be calculated accurately in each situation.

A limited number of reports have been published, using transmission measurements with an external flood source for attenuation correction. These attenuation methods are based on the calculation of an effective attenuation coefficient map to be used in the correction algorithm. Bailey et al. (6) have described a simultaneous dual-window emission and transmission technique where technetium-99m ( $^{99\text{m}}\text{Tc}$ ) ( $h\nu = 140 \text{ keV}$ ) is used for the SPECT study and gadolinium-153 ( $^{153}\text{Gd}$ ) ( $h\nu = 98 \text{ keV}$  and  $103 \text{ keV}$ ) for the transmission study. Malko et al. (7) have used measured, effective attenuation coefficients in an intrinsic attenuation correction algorithm for the evaluation of quantitative liver imaging and have shown the importance of the accurate attenuation correction for accurate analysis of patient data. Recent studies using attenuation coefficient maps has also been published by Manglos et al. (8) and Tsui et al. (9).

It is our belief that instead of using an effective attenuation coefficient  $\mu_{\text{eff}}$ , an appropriate build-up function, combined with a measured density map should be used. The reason is that the build-up function will approach a constant value only at source depths comparable with the thickness of a patient (10). The effective attenuation coefficient map obtained from the transmission measurement will, therefore, not give correction factors that properly correct for the variation in the build-up function at moderate depths.

The aim of this paper is to present an attenuation correction method for quantitative SPECT using measured density maps of the object and Monte-Carlo simulated build-up functions.

## MATERIALS AND METHODS

### Transmission Measurements

The transmission measurement must be performed prior to the SPECT study, to eliminate the contribution from

photons emitted from the administered radionuclide. To produce the density map, two sets of projection data are acquired. The first acquisition is a "blank" study without the object in place. The second is the transmission study with the object situated between the flood source and the scintillation camera. The transmission study and the "blank" study thus represent  $\Phi$  and  $\Phi_0$ , respectively, in Equation 1. A projection  $P_\rho(\theta, r)$ , describing the density distribution for a transverse slice corresponding to a certain position on the object, can then be calculated from:

$$P_\rho(\theta, r) = C \cdot \ln \left[ \frac{\Phi(\theta, r)}{\Phi_0(\theta, r)} \right], \quad (3)$$

where  $\Phi(\theta, r)$  is a projection set from the acquisition study when the object is in place,  $\Phi_0(\theta, r)$  is a projection set from the "blank" study. The acquisition parameters for the "blank" study must be identical to the transmission study and is also compensating for nonuniformities introduced into the projection data when the scintillation camera is rotated.

Equation 3 is applied on all projections measured, and the density projections obtained are then reconstructed to give a density map  $\rho(i, j)$  by using the ordinary SPECT software.

The value of the scaling factor  $C$  was determined in a calibration measurement, with a transmission study of a homogeneous water phantom, giving the density of water in the reconstructed density map. It is important that  $C$  is calculated using identical acquisition parameters to those used for the transmission study and the "blank" study, since the factor  $C$  also includes reconstruction parameters.

### The Attenuation Correction Algorithm

The correction algorithm is based on correcting the measured projection sets  $P_E(\theta, r)$  by applying an individual attenuation factor  $K(\theta, r)$ , where  $r$  is an index for a ray in the projection set defined for a projection angle  $\theta$ . The projection set thus contains projection rays, each of which is the line summation of the activity along the ray  $r$ . The attenuation factor  $K(\theta, r)$  is determined from an uncorrected, reconstructed emission image  $E(i, j)$  and a corresponding density map  $\rho(i, j)$ . For a measured projection set  $P_E(\theta, r)$ , two new projection sets,  $P_{E_u}(\theta, r)$  and  $P_{E_d}(\theta, r)$  are calculated from the emission image  $E(i, j)$ , to estimate the attenuation factor  $K(\theta, r)$ .  $P_{E_u}(\theta, r)$  is an unattenuated projection set, equal to the line summation of the pixel contents  $E(i, j)$  along the ray of view  $\gamma(\theta, r)$  or:

$$P_{E_u}(\theta, r) = \sum_{\gamma(\theta, r)} E(i, j). \quad (4)$$

The other projection  $P_{E_d}(\theta, r)$  is an attenuated projection set obtained by calculating the attenuation of values of each pixel along the ray of view  $\gamma(\theta, r)$  before calculating the line summation or:

$$P_{E_d}(\theta, r) = \sum_{\gamma(\theta, r)} [E(i, j) \cdot B(\mu d) \cdot \exp(-\mu d)], \quad (5)$$

where

$$\mu d = \frac{\mu}{\rho} \cdot \Delta s \cdot \sum_{\gamma(\theta, r)} \rho(i, j). \quad (6)$$

$\mu/\rho$  is the linear mass-attenuation coefficient for a tissue equivalent material corresponding to the energy of the emitted photon, and  $\Delta x$  is the pixel size of  $E(i, j)$  and  $\rho(i, j)$ . The

attenuation factor  $K(\theta, r)$  is calculated from:

$$K(\theta, r) = \frac{P_{Ei}(\theta, r)}{P_{Ea}(\theta, r)}. \quad (7)$$

Emission projections can be acquired in a 180-degree or a 360-degree mode. For a 360-degree mode, the opposite projection sets are averaged by arithmetical mean. Two additional projections  $P_{Eim}(\theta, r)$  and  $P_{Eim}(\theta, r)$  are therefore calculated for the opposite direction. The attenuation factor is in this case calculated from:

$$K(\theta, r) = \frac{P_{Ei}(\theta, r) + P_{Eim}(\theta, r)}{P_{Ea}(\theta, r) + P_{Eim}(\theta, r)}. \quad (8)$$

An unattenuated projection  $P_E'(\theta, r)$  is calculated by multiplying the original, measured attenuated projection ray  $P_E(\theta, r)$  by the attenuation factor obtained  $K(\theta, r)$  or:

$$P_E'(\theta, r) = P_E(\theta, r) \cdot K(\theta, r). \quad (9)$$

Equation 9 is applied for each projection ray  $r$  in the projection set corresponding to the angle  $\theta$ , and for each projection set in the SPECT study.  $P_E'(\theta, r)$  is finally reconstructed to give an unattenuated emission image  $E'(i, j)$ .

### Computer Simulations of the Build-up Function

A determination of the contribution to the projection data from photons, scattered in the object, is necessary. A Monte-Carlo simulation (11) was initiated to obtain an estimate of the build-up function  $B(\mu d)$ , used in Equation 5. Photons, emitted from a 20-cm line source at various depths in a cylindrical phantom (22-cm diameter and 25-cm height) of tissue-equivalent MixD material (elemental composition H (13.40); C (77.79); O (3.50); Mg (3.86); Ti (1.44), density = 0.985 g/cm<sup>3</sup>), were simulated to impinge on a scintillation camera with a parallel-hole collimator. The table of cross-section data for the MixD material was calculated using data from Berger (12). Three different radionuclides, <sup>99m</sup>Tc ( $h\nu = 140$  keV), thallium-201 (<sup>201</sup>Tl) ( $h\nu = 77$  keV) and indium-111 (<sup>111</sup>In) ( $h\nu = 172$  keV, 247 keV) were simulated. The energy window of the detector system was 25%, and the energy resolution was 15% full width at half maximum (FWHM). The energy window was centered around the photo-peaks (the 247 keV peak for <sup>111</sup>In). The events, obtained in a pixel (size = 0.63 cm) in the simulated image matrix corresponding to the mid-point of the line source, were separated into a primary part,  $\Phi_p$ , and a scattered part,  $\Phi_s$ . The build-up function was then calculated as a function of the product  $\mu d$  from:

$$B(\mu d) = \frac{\Phi_p(\mu d) + \Phi_s(\mu, x, y, z)}{\Phi_p(\mu d)}, \quad (10)$$

where  $d$  is the depth of the line source in the simulated phantom. A multiple regression analysis was initiated and a second order polynomial equation  $A_0 + A_1 \cdot \mu d + A_2 \cdot (\mu d)^2$  was fitted to the simulated, build-up data points. The polynomial coefficients  $A_0$ ,  $A_1$  and  $A_2$  were; 1.0267, 0.1845, -0.0197 for <sup>99m</sup>Tc, 1.0480, 0.2276, -0.0275 for <sup>201</sup>Tl, and 1.0166, 0.1692, -0.0190 for <sup>111</sup>In. The multiple correlation coefficients for the polynomial curve fitting for <sup>99m</sup>Tc, <sup>201</sup>Tl and <sup>111</sup>In were calculated to be 0.991, 0.989 and 0.990, respectively. The simu-

lated build-up points and the corresponding polynomial curves are presented in Figure 1.

### Phantom Measurements

To evaluate the usefulness of the attenuation correction method to quantify the radioactivity in a realistic, clinical situation, studies were made on a human-like, nonhomogeneous, Alderson Rando-phantom (Alderson Research Laboratories, Long Island City, NY). This phantom consists of a human skeleton surrounded by tissue-equivalent Rando plastic (density = 0.985 g/cm<sup>3</sup>,  $\bar{Z} = 7.30$ ) and lung-equivalent tissue (density = 0.32 g/cm<sup>3</sup>). The phantom is sliced into transverse sections 2.5 cm in thickness. A matrix of holes 0.5 cm in diameter, separated by 3 cm were drilled in each section.

A GE MaxiCamera 400T (Milwaukee, WI) fitted with a low-energy, general-purpose collimator was used for the measurements. The energy resolution was ~15% FWHM for 140 keV photons. A 25% energy window was used for both the transmission and the SPECT acquisitions. The scintillation camera was interfaced to a minicomputer (PDP 11/34, Digital Equipment Corp., Maynard, MA) with an image processing system (Gamma-II Image Processing system, Digital Equipment Corp., Maynard, MA) and tomographic software (SPETS-II Tomographic System, Nuclear Diagnostics, Inc., Stockholm, Sweden). For the transmission measurements, a 185-MBq (5-mCi), solid <sup>57</sup>Co standard flood source (Amersham Sweden AB, Stockholm, Sweden) was mounted directly on the scintillation camera head, at a distance of 50 cm from the collimator surface.

Three phantom studies were performed, using 20-cm line sources of <sup>99m</sup>Tc, <sup>201</sup>Tl, and <sup>111</sup>In at activity concentrations of 0.30 MBq/cm, 0.12 MBq/cm and 0.06 MBq/cm, respectively. For each phantom study, three separate SPECT measurements were made and in each case four line sources were placed in different positions inside the Alderson-phantom. The position of each line source is indicated in Figure 2. The phantom was carefully placed on the camera couch for the SPECT study, to match the same position as for the transmission study. The thickness and the lateral width of the phantom was also checked for both the transmission study and the emission studies, using <sup>57</sup>Co point sources. In addition to the three phantom studies, one study of three line sources in air for each isotope was carried out with the same reconstruction parameters as for the phantom studies.

Data acquisition for both the transmission measurement and the SPECT measurement was made at 64 angles in the 360-degree rotation mode around the phantom, and events were collected in 64×64 matrices. The acquisition time was 25 sec per angle. Correction for the radioactive decay was made for the <sup>99m</sup>Tc study. The opposite projection data were averaged by arithmetical means and reconstructed by filtered backprojection using a smooth Shepp-Logan filter. The slice thickness and the pixel size for the reconstructed images was 1.26 cm and 0.63 cm, respectively. If the density map and the emission image did not correspond to each other, the relative shift was determined and the density map adjusted to the emission image. Regions-of-interest (ROI) were defined for each line source and the count rate in each ROI was determined for the uncorrected images and corrected emission images with and without using the build-up function. The average values of the measured count rate for the line sources in air were determined and used as reference values.

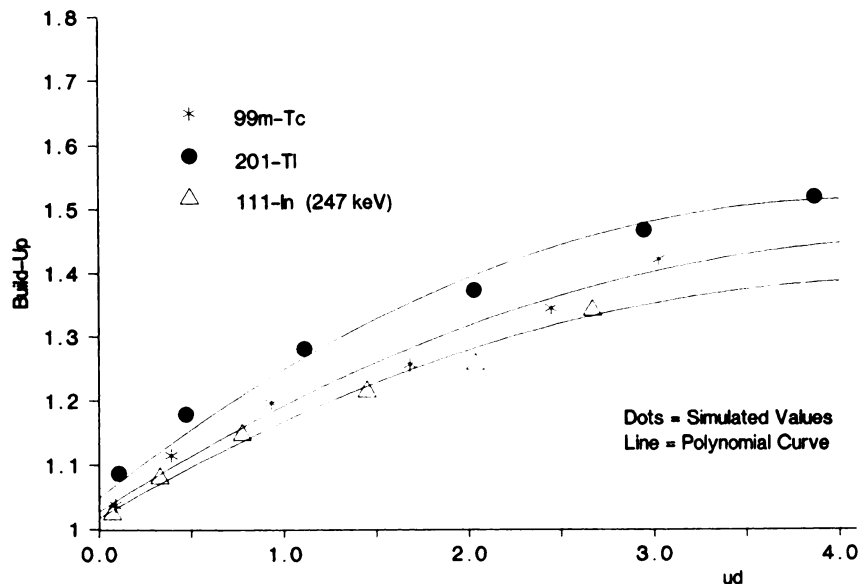


**FIGURE 1**  
The build-up of scattered photons in a pixel has been simulated for three different radionuclides. A second order polynomial has been fitted to the simulated points.

## RESULTS AND DISCUSSION

In Figure 3, a histogram of the measured, average percentage count rates relative to the reference values in air for the uncorrected images, and the corrected emission images using the simulated, build-up functions are shown. The numerical results for the count rates are given in Table 1. The count rates corrected for attenuation for the different line sources should be equal in magnitude, regardless of their position in the phantom, since each line source was filled with the same concentration of radioactivity. As a test of this precondition, the relative difference  $(\text{cps} - \overline{\text{cps}}) / \overline{\text{cps}}$  for the different line sources was calculated, where cps is the count rate for the different line sources and  $\overline{\text{cps}}$  is the average count rate from all line sources. The result is presented in Figure 4.

A small, 16-pixel, ROI was also defined in the centre of the heart (tissue equivalent material) and the lungs in the density map. The measured average density was calculated to be  $0.358 \text{ g/cm}^3$  for the lung and  $0.995 \text{ g/cm}^3$  for the heart. For a 56-pixel ROI, the average density was  $0.371 \text{ g/cm}^3$  and  $0.976 \text{ g/cm}^3$ , respectively. This can be compared with the tabulated values of  $0.32 \text{ g/cm}^3$  and  $0.985 \text{ g/cm}^3$ .

*Technetium-99m.* For the measurement with the  $^{99\text{m}}\text{Tc}$  line sources the average value of the count rate for all line sources in the uncorrected images relative to the air measurement is 38.5%. If an attenuation correction using a mass-attenuation coefficient of  $0.156 \text{ cm}^2/\text{g}$  without including the build-up function is made, the average relative count rate is 123.2%. Using the Monte-Carlo simulated build-up function (I in Fig. 1), the average relative count rate is 105.3%.

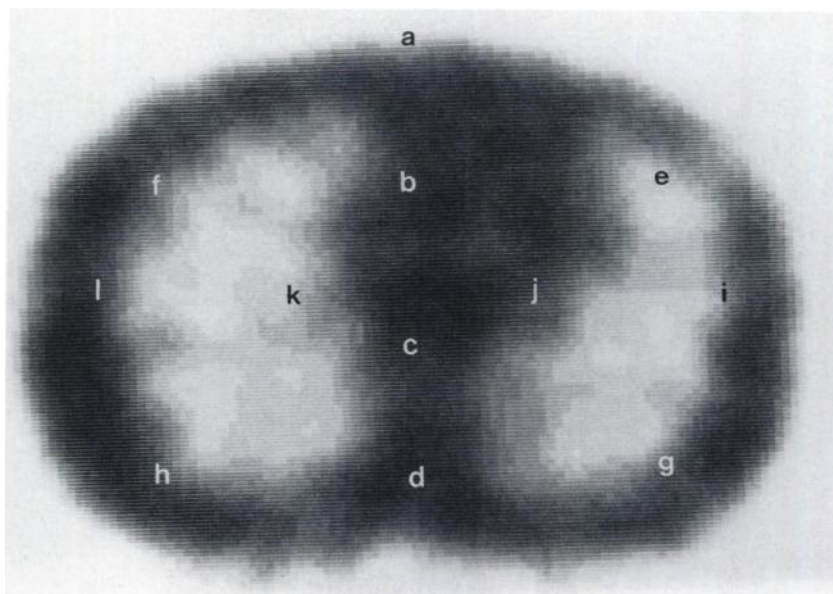


**FIGURE 2**  
This figure shows the measured density map of the Alderson-Rando phantom. The position of the line sources is indicated by the letters a-l. The density map gives a well-defined outline of the object which is important for the attenuation correction.

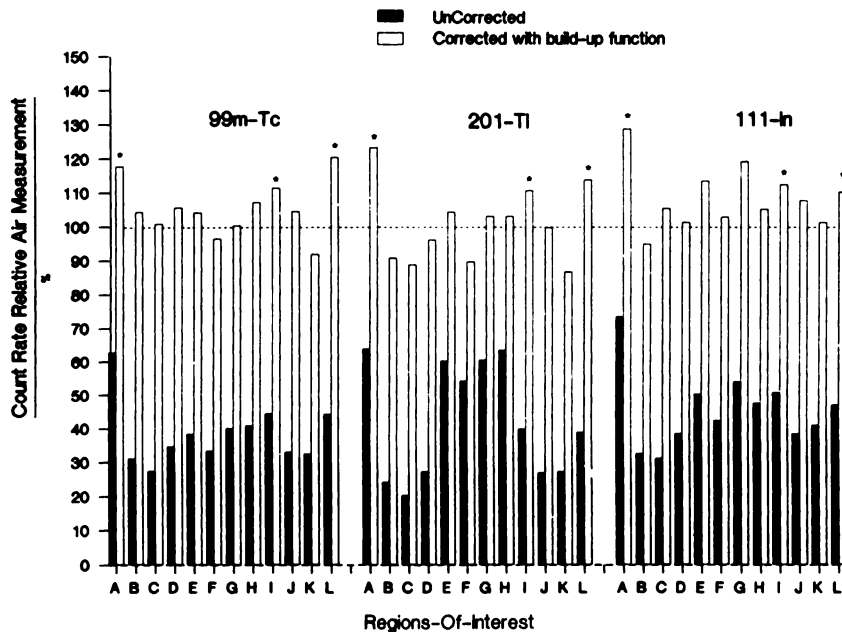


**FIGURE 3**  
Measured count rates for the different line sources A-L relative to the measured count rates in air. The filled bars are corrected for attenuation using the Monte-Carlo simulated build-up function. "\*" indicates sources close to the surface.

**Thallium-201.** For  $^{201}\text{Tl}$  the average relative count rate is 42.2%. This is slightly more than for  $^{99\text{m}}\text{Tc}$ . As in the  $^{99\text{m}}\text{Tc}$  measurement, there is a clear over-correction for the line sources positioned at the surface of the object. If no build-up function is used, the average relative count rate is 23.3% and when the build-up function is used, the average count rate is found to be 100.7%.

**Indium-111.** The average relative count rate for  $^{111}\text{In}$  line sources is 45.4% for uncorrected images, 123.0% for corrected images without using build-up function, and 108.4% for corrected images using the build-up function.

In Figure 2 we can see that line sources A on the surface of the phantom and line sources I and L near the surface are significantly over-corrected. This may be caused by inaccuracy in the build-up function, which is calculated for a source at varying depth of the length-wise axis of a cylindrical phantom. If these three sources are omitted for  $^{99\text{m}}\text{Tc}$ , the average count rate will be 34.5% for the uncorrected images and 120.2% and 101.6% for the corrected image without build-up and corrected image with build-up, respectively. There is, thus, a very good attenuation correction for a source located some distance below the surface. If the three surface sources are not taken into account for  $^{201}\text{Tl}$ , the

**TABLE 1**  
Measured Count Rates and Counting Statistics in Emission Images

Sources	Air	All line sources			Line sources A, I, and L excluded			
		No Corr	Linear $\mu$	Build-up	No Corr	Linear $\mu$	Build-up	
$^{99\text{m}}\text{Tc}$	Mean	85.6	33.0	105.4	90.1	29.5	102.9	87.0
	S.D.	1.0	7.6	6.4	6.7	3.6	4.4	3.9
	S.D./Mean (%)	1.2	23.2	6.1	7.4	12.1	4.3	4.5
	Mean/Air (%)	100.0	38.5	123.2	105.3	34.5	120.2	101.6
	Max-Min	2.4	30.2	26.9	24.3	11.5	13.6	13.1
$^{201}\text{Tl}$	Max-Min/Mean (%)	2.9	91.7	25.5	27.0	39.0	13.3	15.0
	Mean	31.3	13.2	38.6	31.5	12.7	37.2	30.0
	S.D.	0.6	5.1	3.2	3.4	5.4	2.3	2.1
	S.D./Mean (%)	1.9	38.8	8.3	10.7	42.9	6.2	6.9
	Mean/Air (%)	100.0	42.2	123.3	100.7	40.5	118.7	95.7
	Max-Min	1.4	13.6	9.6	11.5	13.5	5.9	5.5
$^{111}\text{In}$	Max-Min/Mean (%)	4.4	103.2	25.0	36.4	106.5	15.7	18.5
	Mean	9.1	4.1	11.2	9.9	3.8	11.0	9.6
	S.D.	3.9	1.0	0.7	0.8	0.7	0.7	0.6
	S.D./Mean (%)	43.4	23.9	6.3	8.1	17.4	5.9	6.4
	Mean/Air (%)	100.0	45.4	123.0	108.4	41.6	120.8	105.5
	Max-Min	0.6	3.8	2.5	3.1	2.1	2.4	2.2
Max-Min/Mean (%)	6.5	93.1	22.8	31.2	54.5	21.4	23.1	

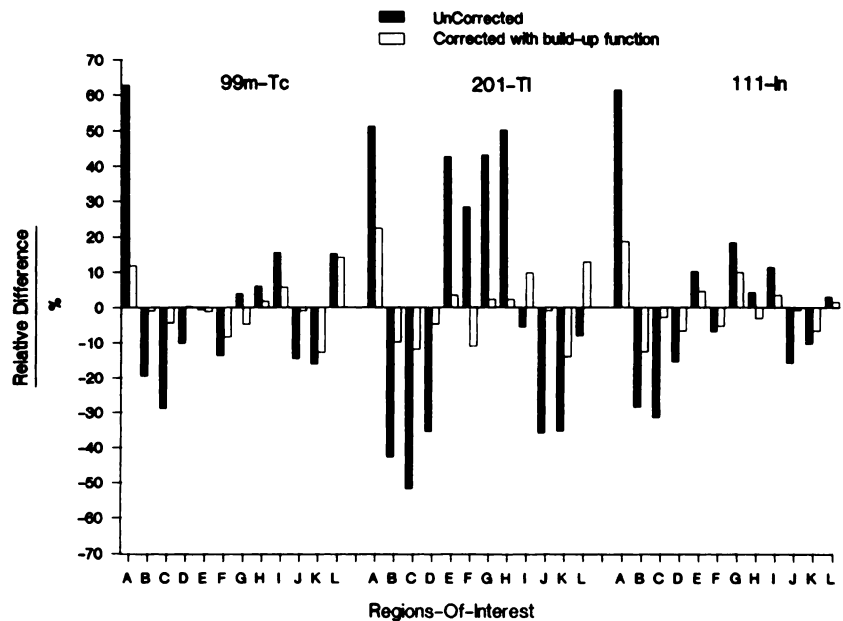


**FIGURE 4**  
The relative difference in count rates (cps-cps)/cps for the line sources in Figure 2.

average relative count rate will be 40.4% for the uncorrected images, 118.7% for attenuation correction using no build-up function and 95.6% using the simulated build-up function. If the surface sources are omitted for  $^{111}\text{In}$  the average count rate values are 41.6%, 120.8%, and 105.5%, respectively.

The SPECT studies for the  $^{111}\text{In}$  line sources have been made using a photo-peak window centered over the 247 keV peak only. This gives reduction in the counting statistics due to the lower sensitivity for the total absorption of the 247 keV photon (the intrinsic efficiency for a NaI(Tl) crystal of 1.27 cm thickness is about 55% for 247 keV photons). A dual-energy window technique could be used, but this should cause problems in the choice of a relevant, mass-attenuation coefficient and the build-up function for the attenuation correction.

The described method is more complicated and time-consuming than most commercially available methods, since a density map has to be obtained. However, this is required for an accurate estimation of the activity. The code has been written so that correction can be made for multiple transverse slices. This provides the possibility of calculating images, corrected for attenuation, other than the transverse slices. The algorithm is of the iterative type, since the image corrected for attenuation  $E'(i, j)$ , reconstructed from the attenuation-corrected projection  $P_E'(\theta, r)$ , can be used as input for a new attenuation correction of the original measured projections  $P_E(\theta, r)$ . An investigation of the convergence criteria is beyond the scope of this work, however.

Since the algorithm is time-consuming, a precalculation of the coordinates corresponding to 128 different projection angles around the object was done and stored in a data file. The time to correct an image by this technique was thus reduced by a factor of 12, to ~1

min per image, in the case of the PDP 11/34 computer.

The basic assumptions when making the density map is that the build-up of photons scattered in the object is nearly constant, since the position of the external flood source is equivalent to a source at a relatively large depth. It is also assumed that the variation of the mass-attenuation coefficient for the different tissues in the object is not significant ( $\mu/\rho$  for 140 keV, 77 keV and 247 keV is 0.157 cm<sup>2</sup>/g, 0.189 cm<sup>2</sup>/g and 0.130 cm<sup>2</sup>/g, respectively for the MixD composition and 0.156 cm<sup>2</sup>/g, 0.220 cm<sup>2</sup>/g and 0.124 cm<sup>2</sup>/g for bone-equivalent material (12). From the results, we can see that there is good agreement between the measured densities and the tabulated Rando-plastic densities. The possibility to determine the density distribution has also been shown by Greer et al. (13) using transmission measurements to investigate the accuracy in measuring density distribution with a SPECT system.

A standard, solid,  $^{57}\text{Co}$  flood source can be used independently of the radionuclide being administered, since the purpose of the transmission measurement in our method is to determine the density distribution. The source is commercially available and can be mounted on the camera quickly and easily. Thus, an overall reduction in time when making the transmission study can be achieved. This is of great importance for routine clinical studies. The statistical accuracy in the density map will increase, with increasing radioactivity in the flood source. The activity in the flood source is, however, limited by count-losses and mispositioning of events in the scintillation camera (14). The highest count rate is measured in the "blank" study, since the object attenuates photons. However, if the daily variation in uniformity of the scintillation camera being used is not significant, a standard blank study could be used. The blank study must, however, be scaled to the partic-

ular transmission study. If a standard blank study is used, the activity in the flood source for the transmission study could be increased and the time for producing a density map further reduced.

The work by Bailey et al. (6) is interesting, since the transmission study and the emission study are carried out simultaneously. The major advantage is that no additional transmission data acquisition is required, thus increasing the possibility for accurate attenuation correction in routine clinical studies. The contribution from  $^{99m}\text{Tc}$  photons scattered into the  $^{153}\text{Gd}$  window is, however, a problem and has been estimated by using a convolution scatter correction technique.

The density maps could also be obtained with an x-ray CT scanner. The CT maps have high resolution and the statistical uncertainty in the density coefficients is very low. The external flood source technique gives density maps of lower spatial resolution and statistical accuracy. It is, however, our belief that the flood source method is preferable due to its simplicity and availability.

An accurate definition of outline of the object is essential for the attenuation compensation. One simple method is to approximate the outline to an ellipse where the major and minor axes are equal to the thickness and the lateral width respectively (4). This approximation can give inaccurate attenuation compensation in regions where the outline is not elliptical, such as the thorax for females. The definition of the outline as a single ellipse is also used as a common outline for all sections of the object. Other authors (15,16) have presented methods using dual-windows to obtain reconstructed images of scattered photons which then serves as a base for the outline definition. The outline can, however, be very accurately obtained from a transmission measurement of the object. The attenuation coefficients obtained outside the object are very close to zero and the outline is therefore easy to define. Each attenuation map also defines an outline matching the corresponding section of the object.

In summary, the correction for photon attenuation in SPECT studies has received much attention in the literature in the past years. Due to its complexity, no general solution has been presented. For this reason, SPECT has up to now been used mostly for qualitative studies. It is, however, essential to compensate for photon attenuation even in qualitative studies, since photon attenuation in nonhomogeneous regions affects the spatial distribution of events in the reconstructed image. Furthermore, this effect increases when radionuclides that emit low-energy photons are used, e.g.,  $^{201}\text{Tl}$  used in myocardial studies. This paper shows that it is possible to quantify total activity in different parts of an object with a high degree of accuracy for different types of radionuclides.

The correction method, described here, is based on

using simulated build-up functions when correcting for contribution from scattered photons. The method was applied to SPECT measurements with a well-defined geometry and source distribution. Since the build-up of scattered photons in the acquired projection image is truly a three-dimension problem and that the described method, using Monte-Carlo simulated functions, is a first attempt to define the scope of the problem, further investigations and developments must be made to test the validity of the method on complex source distributions.

Since the simulated build-up functions are valid for a cylindrical, homogeneous phantom, our future aim is to implement a scatter correction technique (17) that uses data from nonhomogeneous phantoms. This is necessary in order to overcome the problems when correcting for attenuation in different attenuating media or near the boundary. In clinical research, we are planning the further development of the attenuation correction for its application in a dose-planning system for internal radionuclide therapy (18). Calculation of absorbed dose in radionuclide therapy have been shown to be less accurate than those made in external radiation therapy. Proper dose planning requires an absolute quantification of the uptake of the therapeutic radiopharmaceutical (19). The possibility to estimate the activity in nonhomogeneous areas of the object, made available by attenuation correction, is very promising and it should be possible to estimate the absorbed dose in the target volume to an accuracy comparable to those in external beam therapy.

#### ACKNOWLEDGMENTS

This work was supported by grants from the Swedish Cancer Foundation, Grant No. 2353-B87-01XA, the John and Augusta Person Foundation for Scientific Research, Lund; the Royal Physiographic Society, Lund; the Medical Faculty of Lund, and Mrs. Bertha Kamprad's Cancer Foundation. This work was presented in part at the SNM 33rd Annual Meeting, Washington, DC 1986 (20).

#### REFERENCES

1. Jaszczak RJ, Coleman RE. Single photon emission computed tomography (SPECT) principles and instrumentation. *Invest Radiol* 1985; 20:897-910.
2. Coleman RE, Blinder RA, Jaszczak RJ. Single photon emission computed tomography (SPECT): clinical applications. *Invest Radiol* 1986; 21:1-11.
3. Siegel AS, Wu RK, Mauer AH. The buildup factor: effect of scatter on absolute volume determination. *J Nucl Med* 1985; 26:390-394.
4. Larsson SA. Gamma camera emission tomography: development and properties of a multi-sectional emission computed tomography system. *Acta Radiol Suppl* 1980; 363:1-75.
5. Chang LT. A method for attenuation correction in radionuclide computed tomography. *IEEE Trans Nucl Sci* 1978; 25:638-643.
6. Bailey DL, Hutton BF, Walker PJ. Improved SPECT using

- simultaneous emission and transmission tomography. *J Nucl Med* 1987; 28:844-851.
7. Malko JA, Van Herten RL, Gullberg GT, et al. SPECT liver imaging using an iterative attenuation algorithm and an external flood source. *J Nucl Med* 1986; 27:701-705.
  8. Manglos SH, Jaszczak RJ, Floyd CE, Hahn LJ, Gree KL, Coleman RE. Nonisotropic attenuation in SPECT: phantom test of quantitative effects and compensation techniques. *J Nucl Med* 1987; 28:1684-91.
  9. Tsui BMW, Gullberg GT, Edgerton ER, et al. Correction of nonuniform attenuation in cardiac SPECT imaging. *J Nucl Med* 1989; 30:497-507.
  10. Siegel JA, Wu RK, Mauer AH. The buildup factor: effect of scatter on absolute volume determination. *J Nucl Med* 1985; 26:390-394.
  11. Ljungberg M, Strand S-E. A Monte Carlo program for the simulation of scintillation camera characteristics. *Comput Meth Prog Biomed* 1989; 29:257-272.
  12. Berger MJ, Hubbell JH. XCOM: photon cross sections on a personal computer NBSIR 87-3597. National Bureau of Standards, 1987.
  13. Greer KL, Harris CC, Jaszczak RJ, et al. Transmission computed tomography data acquisition with a SPECT system. *J Nucl Med Technol* 1987; 15:53-56.
  14. Strand S-E, Larsson I. Image artifacts at high photon fluence rates in single-crystal NaI(Tl) scintillation cameras. *J Nucl Med* 1978; 19:407-413.
  15. Gullberg GT, Malko JA, Eisner RL. Boundary definition. In: Eisner RL, ed. *Emission computed tomography—current trends*. New York: Society Nuclear Medicine; 1983:33-53.
  16. Huang S-C, Carson RE, Phelps ME, et al. A boundary method for attenuation correction in positron computed tomography. *J Nucl Med* 1981; 22:627-637.
  17. Axelsson B, Msaki P, Israelsson A. Subtraction of compton-scattered photons in single-photon emission tomography. *J Nucl Med* 1984; 25:490-494.
  18. Ljungberg M, Strand S-E. Dose planning with SPECT. *Int J Canc Suppl* 1988; 2:67-70.
  19. Strand S-E, Norrgren K, Ingvar C, et al. Parameters required in a dose planning model for radioimmunotherapy. In: Schabiger PA, Hasler PH, eds. *Radionuclides for therapy*. Villigen Switzerland: Bottsteiner Colloquium IC; 1986:75-90.
  20. Ljungberg M, Strand S-E, Jonson B. Iterative attenuation correction in SPECT using attenuation coefficients obtained from transmission measurements [Abstract]. *J Nucl Med* 1986; 27:1004.